

O₂/N₂ mixtures under pressure: A structural study of the binary phase diagram at 295 K

D. Sihachakr and P. Loubeyre

DIF/Département de Physique Théorique et Appliquée, CEA, Boîte Postale 12, 91680 Bruyères-le-Châtel, France

(Received 11 May 2004; revised manuscript received 24 June 2004; published 15 October 2004)

The binary phase diagram of O₂/N₂ mixtures has been measured at 295 K up to 14 GPa in a diamond anvil cell. The boundary lines and the structures of the various solid phases have been determined by the combination of visual observation of the phase transitions, synchrotron x-ray diffraction, and Raman spectroscopy. A large substitution of O₂, up to 20%, in solid N₂ does not modify the sequence of structures observed in pure N₂ solid. On the other hand, only less than 5% of N₂ can be substituted in solid O₂. Five structures of O₂/N₂ solid solutions have been identified. In particular, a continuous solid solution obtained by substitution of O₂ molecules in the δ -N₂ phase is observed to extend up to 95 mol% O₂. Deviation from pure random substitution is observed. Also, evidence of the existence of two compounds, (N₂)₃O₂ and N₂(O₂)₂, are discussed.

DOI: 10.1103/PhysRevB.70.134105

PACS number(s): 62.50.+p, 64.75.+g, 78.70.Ck, 78.30.-j

I. INTRODUCTION

O₂ and N₂ are two homodiatom molecules that contain multiple bonds and O₂ is the only diatomic molecule to carry a magnetic moment. Hence, numerous theoretical and experimental works have been devoted to investigate high-pressure effects on molecules in pure oxygen and pure nitrogen.¹ Up to 10 GPa, in both systems, a rich polymorphism has been revealed due to the interplay between quadrupolar forces, magnetic interaction, the ratio of the molecular bond length over the intermolecular distance, or pairing of molecules. In the 100 GPa range, new structures have been recently identified when chemical changes become dominant, as with the formation of oxygen metal² or of nonmolecular phases of nitrogen.³ The study of oxygen and nitrogen under pressure is also of direct relevance to understand the physical and chemical processes in condensed phases with application to planetary physics, detonation of high-energy materials, and the synthesis of novel materials by pressure.⁴ Atomistic modeling can provide valuable information regarding these applications but it is then important to have a reliable force field between the molecular entities. High-pressure equation of state data have been shown useful to refine these force fields.⁵

For the understanding of fundamental pressure effects on molecules or its application to natural phenomena, the study of O₂/N₂ mixtures under pressure should be as interesting as the ones of pure systems. In particular, the binary phase diagram is a sensitive test of the binary interactions. Furthermore, studies of mixtures of simple molecules at high pressure has revealed a number of interesting phenomena, such as the existence of Van der Waals compounds.^{6,7} Yet, few theoretical and experimental studies have been devoted to the properties of O₂/N₂ phase diagram under pressure or the chemical changes induced by pressure in these mixtures. Only three studies have been reported in the literature on O₂/N₂ mixtures under pressure.⁸⁻¹⁰ Baer and Nicol⁹ have determined by Raman scattering at 295 K indirectly parts of the *P*-*x*% binary diagram. It was shown that the components were highly miscible below 9.5 GPa in the β -O₂ and δ -N₂ solid phases.

The aim of the present study is to do a complete and direct determination of the boundary lines of the binary phase diagram and a structural determination of the O₂/N₂ solid mixtures. The following questions will then be addressed: How does the solubility of one component in the solid of the other modify the sequence of phase transitions of the pure components? Are there new structures for the O₂/N₂ alloys? Does Van der Waals compounds exist? What is the excess volume of mixing? The outline of the paper is the following: in Sec. II, experimental details are presented; in Sec. III, the phase diagram is constructed and the structural determination presented; in Sec. IV, comparison with previous determinations and the analysis of the data are discussed.

II. EXPERIMENT

The membrane diamond anvil cell has been used for generating the static high pressure. In previous studies, we have shown that this device is well adapted for measuring the properties of binary mixtures at high pressure.^{7,11} Since the pressure in the sample chamber can be finely varied by controlling the force on the piston through the gas pressure on the membrane, phase transitions can be probed at constant temperature. Also, the diamond anvil cell (DAC) is loaded at room temperature in a high-pressure vessel, typically under a pressure of 20 MPa to avoid the use of a compressor that can be dangerous with oxygen. BeCu gaskets were used to confine the sample and the sample chamber at 10 GPa was typically 100 μ m in diameter and 30 μ m thick. The concentration of the sample is calculated from the partial pressures of the initial mixtures (stabilized for at least 12 h in the loading vessel) corrected with the second virial coefficients. The error bar on the concentration is less than 1%. A total of 20 different initial concentrations have been studied and measurements at some concentrations were repeated a few times to test reproducibility. The pressure was measured with the ruby luminescence technique using the quasihydrostatic ruby scale.¹² The error bar in pressure is ± 0.05 GPa.

Phase transitions boundary lines of the O₂/N₂ phase diagram, as presented in Fig. 1, have been clearly detected by visual observation through a microscope apparatus associ-

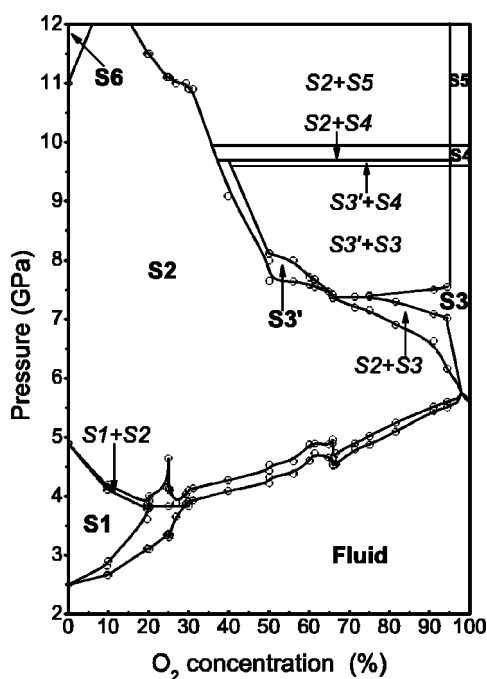


FIG. 1. Binary phase diagram of O_2/N_2 at 295 K and up to 12 GPa. \circ are data points determined from visual observation. The lines are interpolated from the data points and drawn to satisfy the Gibbs phase rule.

ated to the pressure measurement. The sample was observed at each point from few minutes to several hours to test for equilibration. During these observations, we did not notice any change of the sample with time. Solid-fluid equilibrium could be easily seen (Fig. 4). At each concentration, the $S+F$ domain extends over a certain pressure range. The transition points were the most finely detected by working with a single crystal in equilibrium with a fluid. The $S+F$ domain is then delimited by the locus of the $P(x)$ points when the small single crystal was seen to disappear and when the single crystal is seen to fill the whole sample chamber. The transition between the various structures of O_2/N_2 alloys, as identified by x-ray diffraction and Raman spectroscopy, could be detected by visual observation by following with pressure the changes in a single crystal grown from the melt. Following the labels of Fig. 1, the $S1-S2$ transition could easily be observed because there is a pressure domain over which the two solid phases coexist and a boundary between two single crystals was observed. The $S2-S6$ transition is harder to detect by direct observation or by Raman spectroscopy. This transition is associated to the breakage of the single crystal in few parts and was finally proven by x-ray diffraction where this displacive phase transition can be clearly seen (Fig. 5). The transition from $S2$ to $S2+S3$ is easily detected because it is associated to a change of color and texture of the solid. The transition from $S2$ to $S3'$ is hard to detect because the single crystal is not broken at the transition, however, a transition front is observed to cross the solid. The $S2+S4$ and $S2+S5$ solid-solid phase separations are clearly detected. Figure 2 shows microphotographies of several O_2/N_2 mixtures that point out the different aspects of those mixtures according to the different stability domains.

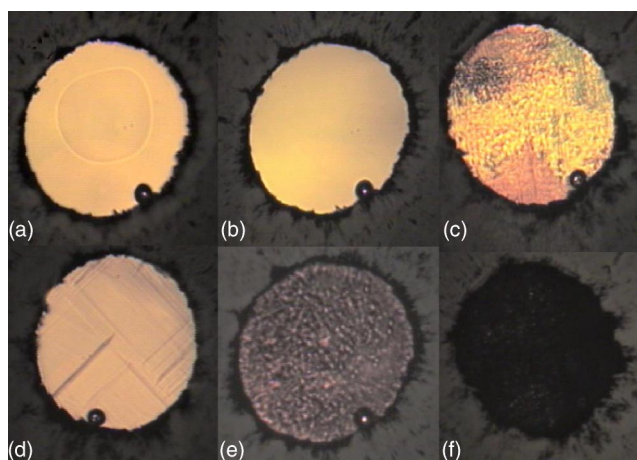


FIG. 2. (Color online) Microphotographies of several N_2/O_2 mixtures at different pressures and concentrations: (a) $S2$ -fluid equilibrium at 4.2 GPa for N_2/O_2 mixture with 50 mol% O_2 . (b) $S2$ phase at 5 GPa for a N_2/O_2 mixture with 50 mol% O_2 . (c) $S2+S3$ equilibrium at 6.7 GPa for N_2/O_2 mixture with 80 mol% O_2 . (d) $S3+S3'$ equilibrium at 7.5 GPa for N_2/O_2 mixture with 66 mol% O_2 . (e) $S2+S4$ equilibrium at 9.4 GPa for N_2/O_2 mixture with 50 mol% O_2 . (f) $S2+S5$ equilibrium at 12 GPa for N_2/O_2 mixture with 80 mol% O_2 .

The structures of the O_2/N_2 alloys have been measured by synchrotron x-ray diffraction at the ESRF using angle dispersive monochromatic x-ray diffraction at 0.3738 \AA (ID30) and at 0.417956 \AA (ID09). The diffracted signal has been recorded on a MAR3450 imaging plate system, located at a distance of $\approx 400 \text{ mm}$ from the sample. The diffraction geometry was determined using a Silicon reference sample. Maximum 2θ value was 23° . A DAC equipped with boron seats was used to have a large x-ray aperture. The DAC was rotated by $\pm 12^\circ$ to have access to a sufficient fraction of the reciprocal space when the sample was a single crystal. Diffraction images were scanned with $100 \mu\text{m}$ spatial resolution and integrated using the Fit2D software.¹³ Powder spectra have been analyzed using Datlab, and the lattice parameters optimized taking into account all diffracted peaks. Single-crystal diffracted peaks were individually integrated after refinement of the beam center. No evidence of nonhydrostatic compression could be evidenced with these two analysis. Absolute uncertainty in the lattice parameter is at maximum 10^{-3} . Five different concentrations have been studied, respectively, 10, 25, 50, 66, and 75 mol% O_2 , in order to cross all the domains of stability of the various solid phases identified in the phase diagram below 14 GPa. In all cases, the pressure evolution started from the single crystal grown from the melt. Also, by working with a single crystal, it could be seen whether the phase transitions under pressure are displacive, i.e., keeping the single crystal, or reconstructive, i.e., leading to a powder-diffraction pattern. Furthermore, Raman spectroscopy was performed in several places of the sample to verify homogeneity of the single-crystal composition. We did not observe any deviation of the concentration across the crystal.

Finally, Raman spectroscopy was also performed to confirm direct visualization. In $S1$, $S3$, $S3'$, $S4$, and $S5$, one

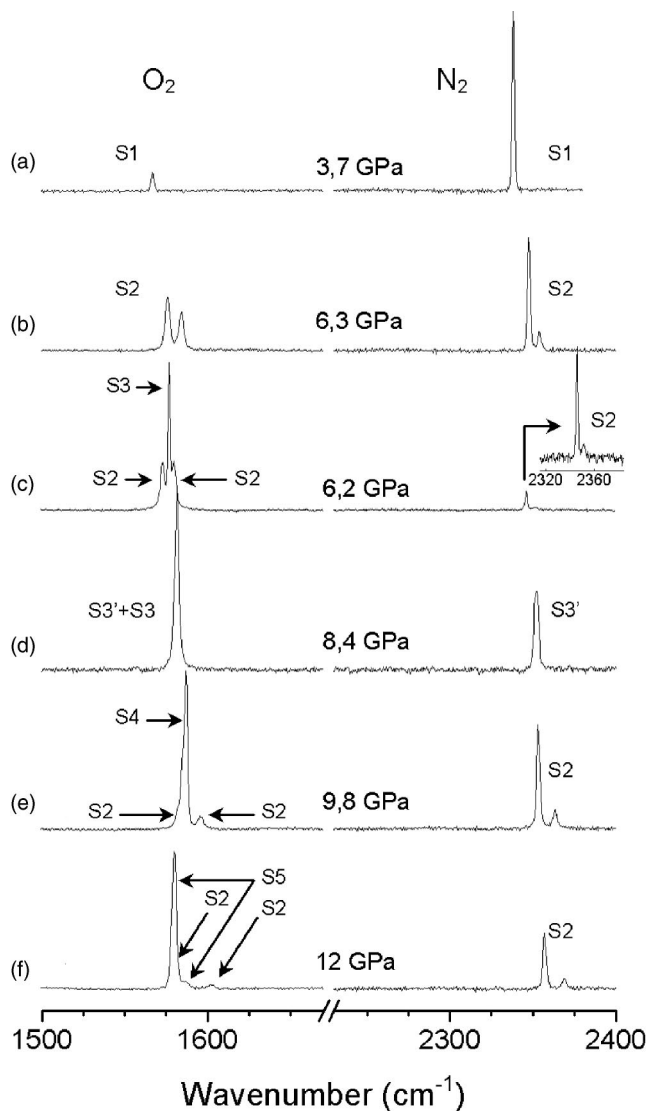


FIG. 3. Raman spectra of several N₂/O₂ mixtures at different pressures and concentrations. The spectra correspond to (a) S1 phase at 3.7 GPa from a N₂/O₂ mixture with 10 mol% O₂. (b) S2 phase at 6.3 GPa from a N₂/O₂ mixture with 50 mol% O₂. (c) S2+S3 phases at 6.2 GPa from a N₂/O₂ mixture with 94 mol% O₂. (d) S3+S3' phases at 8.4 GPa from a N₂/O₂ mixture with 66 mol% O₂. (e) S2+S4 phases at 9.8 GPa from a N₂/O₂ mixture with 50 mol% O₂. (f) S2+S5 phases at 12 GPa from a N₂/O₂ mixture with 50 mol% O₂.

vibron peak for O₂ and for N₂ is observed whereas in S2 and S6, two vibron peaks for both molecules are observed. Typical Raman spectra that were obtained for N₂/O₂ mixtures in the different stability domains are presented in Fig. 3. The detailed Raman spectroscopy of the vibron frequency and width of the O₂ and N₂ vibrons with pressure and concentration has been done in a previous study⁹ and that is essentially confirmed in the present work. Raman spectra were obtained with a 514 nm Ar laser line excitation and a XY 500 DILOR spectrograph equipped with a charge-coupled device detector.

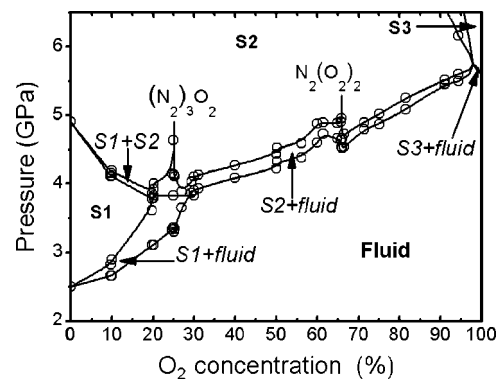


FIG. 4. Enlargement of the solid+fluid domain. \circ are data points determined from visual observation. The lines are interpolated from the data points and drawn to satisfy the Gibbs phase rule. At 25 and 66 mol% O₂ irregularities show evidences of the presence of two compounds, (N₂)₃O₂ and N₂(O₂)₂, as discussed in the text.

III. RESULTS

A. Binary phase diagram

The O₂/N₂ binary phase diagram at 295 K is given in Fig. 1, as obtained from visual observation and Raman measurements. Many transition data points have been measured and the boundary lines have been drawn to connect those points on the basis of Gibbs phase rule. The solid phases, number from S1 to S6, as supposed to be related to the structures of pure O₂ and pure N₂ phase diagram. This will be directly proven below from the analysis of the x-ray diffraction measurements. Two important features of the phase diagram have been already pointed out from a previous Raman study:⁹ there is a total miscibility in the fluid phase; there is a large miscibility of O₂ in the the δ -phase of solid N₂, S2. But the larger number of concentrations studies in the present study, the greater accuracy in the determination of the concentration and of the pressure of phase transitions, enables to observe finer details and other features of the phase diagram.

The range of solubility of N₂ in solid O₂ is small, less than 5 mol%, apart from a domain around 7 GPa. A new structure S3' is observed in a domain at the center of the diagram and not connected to the structure of the pure components. In this case, x-ray diffraction was necessary to show the coexistence of the S3 phase with the new S3' phase. Finally, no phase separation is observed at least to 14 GPa, in alloys which contain up to 20 mol% O₂. Also, the liquidus and solidus line have been determined with great detail (Fig. 4). The solidus line presents discontinuities at 25 and 66 mol% O₂. The liquidus line presents associated peritectic points at O₂ concentrations slightly higher than the discontinuities on the solidus line. These modifications from a regular spindle-type phase diagram is suggesting the existence of two compounds, (N₂)₃O₂ and N₂(O₂)₂, which have incongruent melting. These possibilities have been tested by x-ray diffraction as explained in the following section.

B. Structures of the alloys

The structures of pure solid N₂ and pure solid O₂ under pressure have been extensively studied and in both cases a

rich polymorphism has been observed. At 295 K, O_2 exhibits four stable phases.^{14,15} O_2 solidifies at 5.5 GPa in the rhombohedral β - O_2 magenta phase with space group¹⁶ $R\bar{3}m$ and one molecule per cell. With increasing pressure, a phase transition occurs at 9.6 GPa to form the orthorhombic $Fmmm$ δ - O_2 orange phase¹⁷ that contains four molecules per cell. This phase is stable up to 9.9 GPa where it transforms into the ϵ - O_2 phase that is monoclinic with $C2/m$ space group¹⁸ and eight molecules per cell. The ϵ - O_2 phase is stable up to 96 GPa where O_2 becomes a metal.¹⁹ At 295 K, N_2 exhibits the following sequence of solid phases. N_2 solidifies at 2.49 GPa into the hexagonal close-packed and orientationally disordered β - N_2 phase with space group $P6_3/mmc$.^{21,20} At 4.9 GPa, it transforms into the δ - N_2 cubic phase with space group $Pm\bar{3}n$.^{22,23} The cubic δ - N_2 cell contains eight molecules distributed on two different crystallographic sites. Two orientationally disordered molecules are located at the a sites (the corners and the center). Six disklike disordered molecules are located at the c sites (positioned perpendicularly in pairs at the faces of the cell). This phase is stable up to 11 GPa where it transforms into the δ_{loc} - N_2 phase²⁵ that seems to be a distortion of the δ - N_2 phase. Synchrotron x-ray experiment gives δ_{loc} - N_2 a tetragonal structure with 16 molecules per cell and presumably $P4_2/ncm$ space group. Then, at 16.5 GPa, the transition to the rhombohedral ϵ phase takes place.²⁴⁻²⁶ As a consequence, a similar rich polymorphism is expected for the binary O_2/N_2 solids.

Five concentrations have been studied by x-ray diffraction. On the one hand, the structures of all the stable O_2/N_2 alloys observed in the binary phase diagram at 295 K were identified by the sequences of transitions observed under pressure at 10 and 66 mol% O_2 . The d -spacings data of the two runs are reported, respectively, in Tables I and II. On the other hand, x-ray studies were performed at 25, 50, and 66 mol% O_2 to probe whether we could see structural changes in the $S2$ phase associated to the discontinuities observed on the solidus curve. First, it should be pointed out that remarkably a great mobility of the O_2 and N_2 molecules in observed in $S1$ and $S2$ phases, rapid recrystallization is observed that drives the rapid growth of a single crystal. Whatever the thermodynamic path, x-ray diffraction patterns in $S1$ and $S2$ phases are always ones of single crystals. This impossibility of growing a fine powder in $S1$ and $S2$ phases prevented us from doing Rietveld refinement to extract the molecular O_2 and N_2 positions in the unit cell.

The sequence of structures, as described in Table I, observed under pressure at 10 mol% O_2 has been identified by the indexing fit of the d -spacing measured. In $S1$ domain, a hexagonal unit cell with two molecules per cell (space group $P6_3/mmc$) accounts for all the peaks observed. The excess volume of mixing was measured to be less than 0.5%.²⁰ $S1$ is thus obtained by a substitution of N_2 molecules by O_2 molecules in the β phase of solid nitrogen. In $S2$ domain, a disordered cubic $Pm\bar{3}n$ with eight molecules in the unit cell, as δ - N_2 , reproduces very well the diffraction data. Above 12 GPa, a tetragonal unit cell is refined with a possible space group $P4_2/ncm$, as in pure solid δ_{loc} - N_2 . The $S2$ - $S6$ phase transition that is hard to detect by direct visualization or Raman spectroscopy is clearly seen by x-ray diffraction.

TABLE I. Sequence of observed d -spacings for N_2/O_2 at 10 mol% O_2 . During increasing pressure, the single crystal remains through phase transitions. $S1$ is hexagonal $P6_3/mmc$ with $a = 3.537 \pm 0.007$ Å and $c = 5.844 \pm 0.007$ Å ($V = 31.658 \pm 0.163$ Å³/molecule) at 3.66 GPa. $S2$ is cubic $Pm\bar{3}n$ with $a = 6.010 \pm 0.007$ Å ($V = 27.135 \pm 0.095$ Å³/molecule) at 6.7 GPa. $S6$ is tetragonal (possible space group $P4_2/ncm$) with $a = 8.075 \pm 0.007$ Å and $c = 5.694 \pm 0.007$ Å ($V = 23.205 \pm 0.069$ Å³/molecule) at 14.6 GPa.

hkl	d_{obs} (Å)	$d_{obs} - d_{calc}$	hkl	d_{obs} (Å)	$d_{obs} - d_{calc}$
$S1$ at 3.66 GPa					
0 1 0	3.0645	0.0014	0 2 1	1.4810	-0.0005
0 1 1	2.7013	-0.0117	0 2 2	1.3586	0.0021
1 1 0	1.7684	-0.0001	0 1 4	1.3186	-0.0001
0 2 0	1.5324	0.0008			
$S2$ at 6.7 GPa					
0 0 2	3.0051	0.0001	1 0 4	1.4573	-0.0003
1 1 2	2.4533	-0.0003	1 1 4	1.4163	-0.0003
2 2 2	1.7352	0.0003	2 1 4	1.3110	-0.0005
2 1 3	1.6056	-0.0006	2 2 4	1.2279	0.0011
0 0 4	1.5024	-0.0001			
$S6$ at 14.6 GPa					
0 0 2	2.8528	0.0060	2 5 1	1.4521	0.0020
1 0 2	2.6929	0.0080	0 0 4	1.4270	0.0036
1 3 0	2.5467	-0.0070	1 0 4	1.4049	0.0031
3 1 1	2.3367	0.0067	1 5 2	1.3874	0.0034
0 2 2	2.3237	-0.0030	2 0 4	1.3447	0.0023
2 3 1	2.0842	-0.0001	0 3 4	1.2573	-0.0010
0 4 2	1.6460	-0.0008	3 1 4	1.2440	0.0007
1 4 2	1.6101	-0.0035	1 6 2	1.2017	-0.0015
4 3 1	1.5527	-0.0011	3 6 1	1.1772	-0.0006
1 3 3	1.5233	0.0000	1 7 2	1.0599	0.0001

Parts of x-ray diffractograms of the $S2$ cubic phase and of the $S6$ tetragonal phase, as presented in Fig. 5, show that the $S2$ - $S6$ phase transition is displacive. Associated integrated peaks are given in Fig. 6. The equation of state of the alloy is compared to the one of pure solid N_2 in Fig. 7. It is seen that the effect of O_2 substitution on the volume is clear in the δ - N_2 phase whereas almost negligible in β - N_2 and δ_{loc} - N_2 phase. The sequence of phase transitions in $(N_2)_{0.9}-(O_2)_{0.1}$ alloy is thus exactly the one of pure N_2 solid, with a δ - N_2 phase slightly more stabilized by O_2 substitution.

The evolution of the d spacings measured under pressure in a solid O_2/N_2 mixture with 66 mol% O_2 probes other domains of the phase diagram, as presented in Table II, and enables one to identify the following sequence of structures. The $S2$ phase, as for a concentration of 10 mol% O_2 , is derived from δ - N_2 by the substitution of N_2 molecules by O_2 molecules. The differences from a pure substitutional alloy for the $S2$ phase will be analyzed in the following section in terms of the excess volume of mixing and in terms of the distribution of the two components on the two crystallographically different sites of the δ - N_2 structure. In the $S3 + S3'$ domain, x-ray diffraction was performed on few single

TABLE II. Sequence of observed d spacings for N₂/O₂ at 66 mol % O₂. With increasing pressure the single crystal remains at $S2 \rightarrow S3+S3'$ phase transition, at the $S2+S4$ and $S2+S5$ powders are formed. The error on the cell parameters is ± 0.007 Å. $S3$ (space group $R\bar{3}m$) is rhombohedral with $a=2.758$ Å and $c=10.200$ Å ($V=22.397\pm 0.129$ Å³/molecule) (hexagonal cell) at 8.3 GPa. $S3'$ is hexagonal with $a=5.630$ Å and $c=12.358$ Å ($V=24.231\pm 0.074$ Å³/molecule) at 8.3 GPa. $S4$ is orthorhombic $Fmmm$ with $a=6.704$ Å, $b=4.248$ Å, and $c=2.958$ Å ($V=21.060\pm 0.106$ Å³/molecule) at 9.8 GPa. $S5$ is monoclinic $C2/m$ with $a=8.096$ Å, $b=5.724$ Å, $c=3.776$ Å, and $\beta=117.26^\circ$ ($V=19.442\pm 0.087$ Å³/molecule) at 12.2 GPa.

hkl	d_{obs} (Å)	$d_{obs}-d_{calc}$	hkl	d_{obs} (Å)	$d_{obs}-d_{calc}$
S2 at 6.6 GPa					
1 0 1	4.1851	0.0103	2 1 3	1.5774	-0.0005
1 0 2	2.6417	0.0014	0 0 4	1.4752	-0.0008
1 1 2	2.4111	0.0008	1 0 4	1.4317	-0.0002
2 0 2	2.0888	0.0014	1 1 4	1.3911	-0.0005
2 2 2	1.7046	0.0003	0 2 4	1.3202	0.0000
2 0 3	1.6372	-0.0003	2 1 4	1.2883	-0.0001
S3 at 8.3 GPa from S3+S3' domain					
0 0 3	3.3931	-0.0069	1 1 3	1.2800	0.0021
1 0 1	2.3170	-0.0086	1 0 7	1.2446	0.0007
0 1 2	2.1550	-0.0080	0 2 1	1.1838	-0.0023
0 0 6	1.6933	-0.0067	2 0 2	1.1622	-0.0006
0 1 5	1.5574	0.0062	1 1 6	1.0689	-0.0021
S3' at 8.3 GPa from S3+S3' domain					
0 0 2	6.1915	0.0121	2 2 0	1.4070	-0.0005
0 0 4	3.0921	0.0024	2 2 2	1.3727	0.0004
1 1 0	2.8138	-0.0012	1 1 8	1.3542	-0.0001
0 1 4	2.6110	0.0012	0 2 8	1.3045	-0.0004
1 1 2	2.5627	0.0010	2 2 4	1.2808	-0.0001
0 2 0	2.4392	0.0013	0 0 10	1.2363	0.0004
0 2 2	2.2676	-0.0002	0 4 0	1.2190	0.0001
1 1 4	2.0812	0.0003	0 1 10	1.1976	-0.0004
0 0 6	2.0606	0.0008	0 4 2	1.1959	0.0000
0 2 4	1.9144	0.0006	1 2 8	1.1838	-0.0001
0 1 6	1.8974	0.0000	2 2 6	1.1620	-0.0001
1 2 0	1.8430	0.0002	0 4 4	1.1341	0.0002
1 2 2	1.7660	0.0000	0 3 8	1.1196	-0.0001
1 1 6	1.6621	-0.0002	2 3 0	1.1186	0.0000
1 2 4	2.5827	0.0000	0 2 10	1.1022	-0.0001
0 2 6	1.5722	-0.0012	2 3 2	1.1009	0.0002
0 3 2	1.5717	-0.0001	0 4 6	1.0491	0.0001
0 0 8	1.5443	-0.0005	2 2 8	1.0406	0.0002
0 1 8	1.4724	-0.0003	1 2 10	1.0264	0.0000
0 3 4	1.4382	-0.0002			
S4 at 9.8 GPa from S2+S4 domain					
2 0 0	3.3582	0.0062	4 2 0	1.3148	-0.0010
1 1 1	2.2834	0.0010	1 3 1	1.2540	-0.0006
0 2 0	2.1247	0.0007	0 2 2	1.2135	-0.0001
2 2 0	1.7953	0.0008	5 1 1	1.1737	-0.0001
4 0 0	1.6759	-0.0001	2 2 2	1.1414	0.0002
3 1 1	1.6433	-0.0008	6 0 0	1.1173	0.0000
0 0 2	1.4790	0.0000	4 0 2	1.1090	0.0000
2 0 2	1.3524	-0.0007			
S5 at 12.2 GPa from S2+S5 domain					
$\bar{1}$ 1 0	4.5031	0.0233	2 0 1	2.0300	-0.0035
0 0 1	3.3538	-0.0027	$\bar{4}$ 0 1	2.0154	-0.0008
$\bar{2}$ 0 1	3.3240	-0.0066	$\bar{2}$ 0 2	1.8901	0.0022
0 2 0	2.8627	0.0008	$\bar{1}$ 3 0	1.8349	-0.0094
1 1 1	2.3734	-0.0068	$\bar{4}$ 0 0	1.8015	0.0023
$\bar{3}$ 1 1	2.3591	-0.0026	$\bar{5}$ 1 1	1.5571	-0.0001
$\bar{2}$ 2 0	2.2428	0.0029	$\bar{3}$ 3 1	1.5381	0.0014
$\bar{3}$ 1 0	2.2185	0.0061	0 4 0	1.4320	0.0010
0 2 1	2.1804	0.0026	$\bar{2}$ 0 3	1.2430	0.0043
$\bar{2}$ 2 1	2.1678	-0.0029	2 2 2	1.1901	0.0000

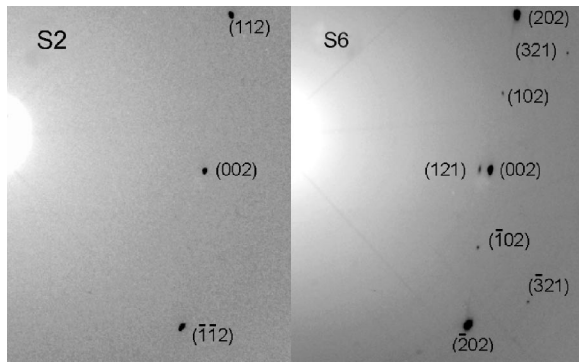


FIG. 5. Parts of x-ray diffractograms of S2 and S6 phases that correspond to 1/10 of an image plate. The x-ray diffraction experiments have been performed at ESRF using angle dispersive monochromatic x-ray diffraction at 0.3738 Å (ID30). The diffracted signal has been recorded on a MAR3450 imaging plate system, located at a distance of ≈400 mm from the sample. For the S2 phase, the x-ray diffractogram corresponds to one single crystal, and for the S6 phase, the x-ray diffractogram corresponds to two single crystals.

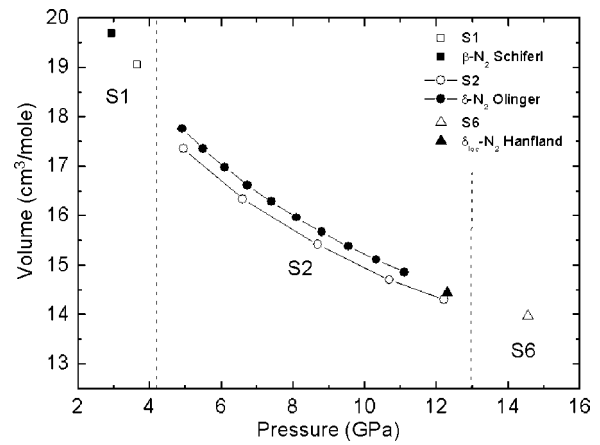


FIG. 7. Equation of state of N₂/O₂ mixture at 10 mol% O₂. The filled symbols correspond to pure N₂ and are from literature (Refs. 20, 22, and 25). The empty symbols are from this study. Dashed lines correspond to phase transitions observed for N₂/O₂ mixture at 10 mol% O₂.

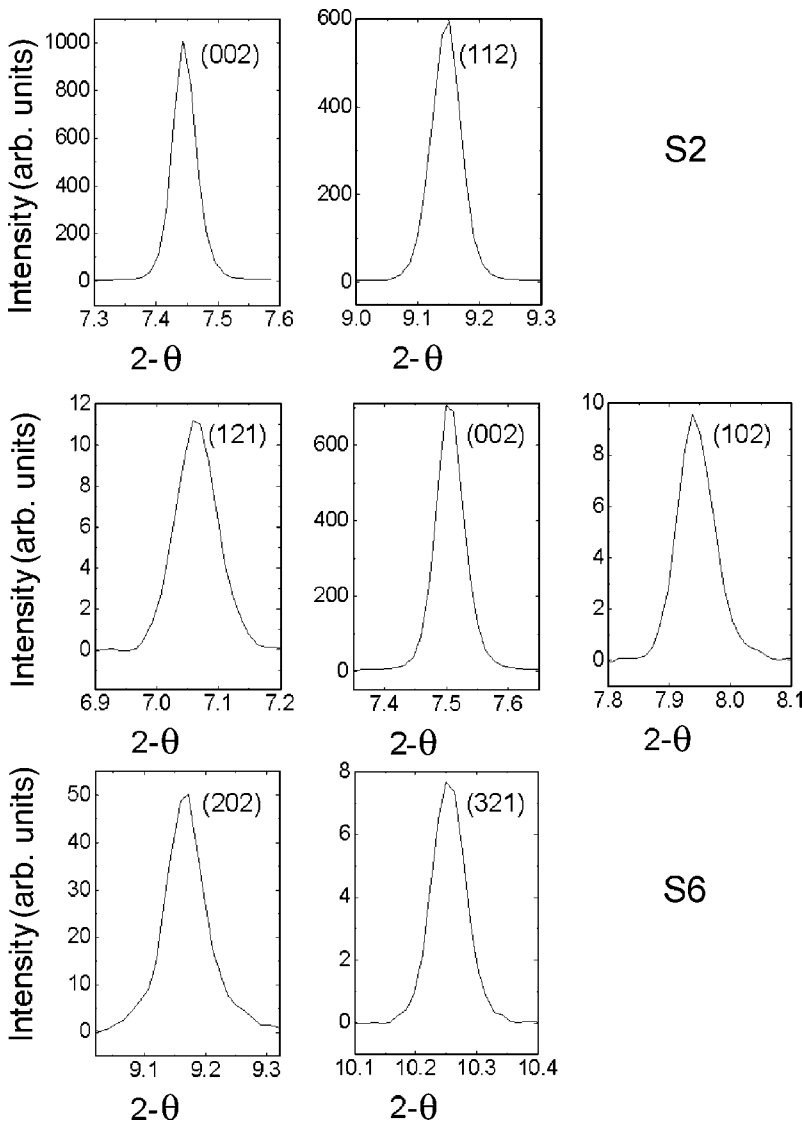


FIG. 6. Integrated peaks of S2 and S6 phases corresponding to the diffracted peaks in Fig. 5.

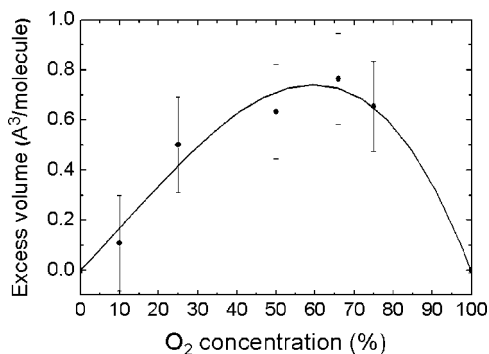


FIG. 8. Evolution of the excess volume with concentration at 6.5 GPa in the *S2* cubic phase. The excess volume is the difference between the present determination of the volume of the solid mixture at a given concentration and the one linearly interpolated for an ideal mixture from the volume of the pure end components.

crystals by increasing pressure from *S2* or on a fine powder by decreasing pressure from *S2+S4*. The diffraction pattern could be refined as corresponding to a mixture of two phases, one, *S3* with a rhombohedral unit cell and a volume very close to the one of β -O₂. *S3* can be described as an hexagonal unit cell with these molecules in it. The other phase, *S3'* has a structure that does not correspond to pure N₂ nor O₂ phases. We best refined the *S3'* structure with a hexagonal unit cell with 14 molecules in it. This structure was also the simplest one that best fits all the diffracted peaks. Moreover, assuming an ideal mixture, we can estimate the concentration of *S3'* to be $\approx 46.5\%$ and this composition is in agreement with the boundary line of the phase diagram. By increasing pressure, x-ray diffraction in the *S2+S4* and *S2+S5* phase-separation domain shows that *S4* is orthorhombic *Fmmm* with four molecules in the unit cell, as δ -O₂ and *S5* is monoclinic with the space group *C2/m* and eight molecules per unit cell, as ϵ -O₂ and their volumes are very close to the ones of the O₂ pure phases.

C. Deviation from ideal substitution in the *S2* phase

As seen in Fig. 1, the *S2* phase covers a large domain of the phase diagram. X-ray measurements at 10 and 66 mol% O₂ have shown that this phase is obtained by substitution of N₂ molecules by O₂ molecules on the sites of the cubic *Pm3n* of δ -N₂. On the other hand, cusp on the solidus curve at 25 and 66 mol% O₂ should indicate deviation from the solid solution at these specific concentrations, i.e., a preferential population of each component on one of the two sites of the structure or a partial order that optimizes the binary or pure interaction energy at these specific concentrations. The Raman measurement of the vibron frequency shift and of the vibron intensity ratio of the two molecules and the x-ray diffraction measurement of the excess volume of mixing versus concentration at a given pressure were performed to address this question. The excess volume of mixing versus the oxygen concentration is plotted in Fig. 8. It is given by the difference between the present x-ray determination of the volume of the solid mixture at a given concentration and the one linearly interpolated from the volume of the pure end

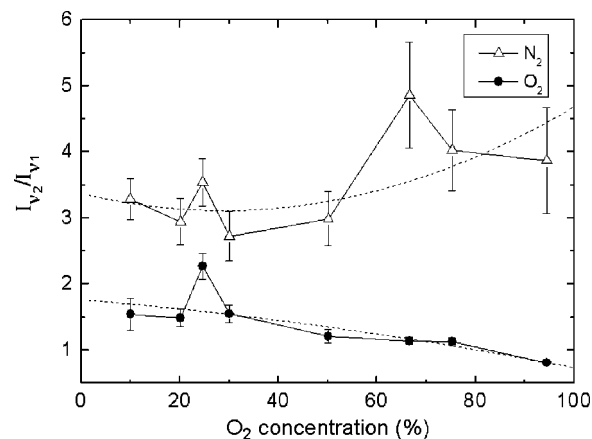


FIG. 9. Evolution of the ratio of the intensity of the two Raman modes of N₂ and O₂ with concentration [$I_{\nu_2}/I_{\nu_1}(x)$] at 6 GPa in the *S2* cubic *Pm3n* phase. This cubic cell contains eight molecules distributed on two crystallographic sites. Two molecules correspond to ν_1 Raman mode, and six correspond to ν_2 Raman mode. Dashed lines are polynomial fit of the data points.

components.^{16,23} It is plotted here at 6.5 GPa but it is seen to be almost independent of pressure. The curve is regular with no indication of more efficient packing at the two concentrations where a deviation from a solid solution is expected.

The Raman spectroscopy measurement of the vibron modes of O₂ and N₂ molecules in the alloy can indirectly probe the microscopic arrangement of the molecules on the crystal lattice. The shift of the vibron frequency is due to the change of the local environment around the molecule that takes place when the volume is varied or the molecular species are changing. The vibron shift should be analyzed as the contribution of two terms, the environmental shift, due to the interaction of the molecule with its surrounding, and the resonance shift, due to an exchange of excitation between identical molecules. Also, the number of vibron modes of a given molecule is related to the number of different crystallographic sites.

The intensity of the different vibron modes is in a first approximation related to the population of the molecules on these different sites. The *Pm3n* structure of the *S2* phase has two crystallographic sites. Thus two vibron modes are measured for O₂ and N₂ molecules.⁹ Each site displays a different type of order. At the (0, 0, 0) and $(\frac{1}{2}, \frac{1}{2}, \frac{1}{2})$ positions of the *Pm3n* unit cell, corresponding to the ν_1 vibron mode, are molecules whose orientations are spherically disordered, while each unit cell face contains two sites at $(0, \frac{1}{4}, \frac{1}{2})$ and $(0, \frac{3}{4}, \frac{1}{2})$ or their equivalents where molecules have disklike orientational distributions, corresponding to the ν_2 vibron mode. There are three times as many disklike disordered molecules as spherically disordered molecules. The intensity of the ν_2 mode should thus be three times the one of the ν_1 mode. In Fig. 9, the ratio of the intensity of the ν_2 mode over the one of the ν_1 , I_{ν_2}/I_{ν_1} , for N₂ and O₂ molecules is plotted versus concentration at 6 GPa. The ratio is around 3 for N₂ and slightly increasing with O₂ concentration. But, it is around 1.5 for O₂ and decreasing with the concentration of O₂. The trend with O₂ concentration, increasing I_{ν_2}/I_{ν_1} for

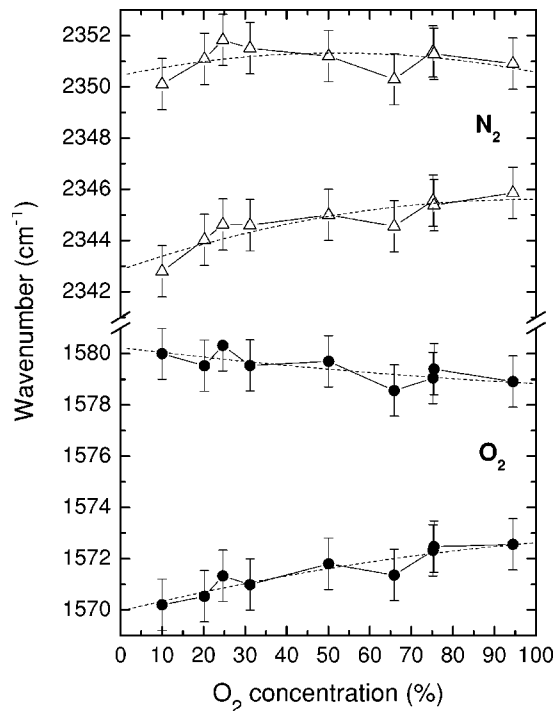


FIG. 10. Evolution with concentration of the frequency of the Raman vibrons of O_2 and N_2 molecules at 6 GPa in the S2 cubic phase. The deviations in the change of the Raman frequencies of O_2 and N_2 vibrons with concentration are correlated to anomalies in the solidus curve (see Fig. 4) and in the evolution of the ratio $I_{\nu_2}/I_{\nu_1}(x)$ (see Fig. 9). Dashed lines are polynomial fit of the data points.

N_2 and decreasing I_{ν_2}/I_{ν_1} for O_2 could suggest that the O_2 molecules slightly prefer to occupy the ν_1 site. That also explains why the ratio is smaller than 3 for O_2 . However, to be more quantitative, if the ratio I_{ν_2}/I_{ν_1} were a correct measure of the distribution of the two components on the sites, we should expect the concentration weighted average value of I_{ν_2}/I_{ν_1} to be 3, instead of the 2.5 value observed in Fig. 9. But it has been explained in the case of $\gamma-O_2$ which is isomorphous to $\delta-N_2$ that the deviation of I_{ν_2}/I_{ν_1} from a factor 3 is due to vibron-vibron resonant transfer coupling.²⁷ Resonant transfer coupling is not important for N_2 . Yet, an important microscopic information of Fig. 9 is thus that O_2/N_2 solid mixtures are not pure random solid solutions. Furthermore, two peaks are observed, in Fig. 9, on the $I_{\nu_2}/I_{\nu_1}(x)$ curves, respectively, at 25 mol% for O_2 molecules and 66 mol% O_2 for N_2 molecules. It is interesting to note that these peaks are correlated to the cusps on the solidus line at these two concentrations. Similarly, the vibron frequency of O_2 molecules and N_2 molecules versus concentration at 6 GPa, as plotted in Fig. 10, seems to show two deviations at 25 and 66 mol% O_2 . This suggests that the site distribution of O_2 and N_2 molecules at 25 and 66 mol% O_2 differs from the concentration trend in solid S2. Hence corroborating the existence of two compounds at these two concentrations. But, due to the complication of vibron-vibron resonant transfer of O_2 molecules, we cannot know quantitatively the relative population of the two molecules on the two lattice sites and whether or not ordered microscopic structures are formed.

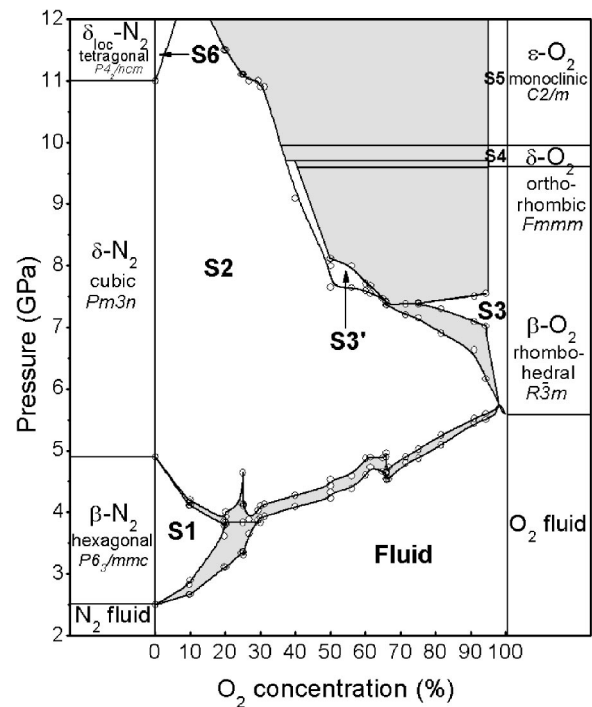


FIG. 11. Comparison between the structures of O_2/N_2 mixtures and the structures of the pure components. Gray domains correspond to phase-separation regions. All the other domains correspond to homogeneous phases. S1, S2, S3, S4, S5, and S6 are isostructural phases of the pure components. S3' is a new homogeneous phase of O_2/N_2 mixtures and has a hexagonal structure that does not exist for pure N_2 or O_2 . A large miscibility of O_2 molecules in N_2 solids is observed, while less than 5% of N_2 can be substituted in O_2 solids.

IV. DISCUSSION

Figure 11 summarizes the P - x miscibility domains of the O_2/N_2 binary phase diagram and how the structures of the solid mixtures are related to the ones of the pure components. For simple interactions between entities, it has been shown that the binary phase diagram could be reasonably predicted in terms of the interactions between the components by an Einstein model for the solid free energy together with perturbation theory for the liquid, as in the case of He/Ne and H_2 He.^{7,28} But the application of the same free-energy calculation is limited here by the ignorance of the O_2-N_2 interaction potential. Also magnetic interaction and possible pairing between O_2 molecules render the problem much more complicated. However, the main trend of the binary phase diagram can be explained by a simple geometrical understanding that relates the shape of the binary phase diagram to the ratio of the effective hard sphere of the two components in the pressure range considered.²⁹ The effective hard-sphere diameters of the two molecular entities can be estimated with the effective pair potential derived from shock-wave Hugoniot.⁵ That gives in O_2/N_2 mixtures around 6 GPa a ratio of $d_{O_2}/d_{N_2}=0.94$. Since this is only slightly different from 1, a large miscibility in the fluid phase and solid phase is expected.

A total miscibility is observed in the fluid phase. A large substitutional miscibility of O_2 molecules in the N_2 solids,

and even an almost complete substitution in the δ -N₂ phase, is observed. In contrast, a very small substitutional miscibility of N₂ molecules in the O₂ solid phases is observed. This dissymmetry of the solubility is very interesting. On the one hand, a large substitutional solubility of O₂ molecules in N₂ solid structures reflects that the O₂-N₂ interaction is quite similar to the N₂-N₂ interaction. But on the other hand, the small solubility of N₂ into O₂ solids indicates that the O₂-N₂ interaction is quite different from the O₂-O₂ interaction. This means that there is a strong deviation from the Lorentz-Berthelot rule for the binary interaction. That could be explained by the importance of the magnetic interaction below 10 GPa that is known to stabilize the O₂ structures observed and by the pairing of O₂ molecules above 10 GPa, known to stabilize the ϵ -O₂ phase. As a consequence, if the magnetic and pairing interaction between O₂ molecules could be turned off, we would probably obtain a complete substitutional miscibility of O₂ in solid N₂ and vice versa, with the sequence of structure of pure N₂ under pressure. The small P - x stability domain of $S3$ and $S3'$, yet over a significant concentration range, is probably ascribed to a subtle interplay of the magnetic interaction in this pressure and concentration range. But the microscopic understanding of it is beyond the scope of the present study.

The present phase diagram is in overall agreement in its major transition lines and shape with the binary phase diagram inferred some years ago from Raman measurements.⁹ But there are large differences in concentration between the two diagrams. The O₂ concentration indirectly estimated from Raman measurement is systematically underestimated and the difference with the present work can amount to 20 mol% O₂. The estimation of the concentration from the Raman intensity is known to be difficult because that requires a careful calibration of the Raman cross section in the condensed phase. This issue is extensively discussed for O₂/N₂ mixtures in a recent work.³⁰ The gas loading of the DAC enables to know directly the concentration of the sample. This error in the determination of O₂ concentration from Raman intensity is also explaining partly why a large miscibility of N₂ in solid β -O₂ has been reported⁹ whereas it is observed to be very small in the present work. The other source of differences stems from the small number of concentrations studied in the investigation of Baer,⁹ in fact insufficient to precisely disclose such a complex binary phase diagram as the O₂/N₂ one.

Two anomalies on the solidus curve and their correlation with ruptures in the evolution versus concentration of the Raman intensities and frequencies of the O₂ and N₂ vibrons in the $S2$ phase, see Figs. 9 and 10, are interpreted as evidences of the existence of two compounds, (N₂)₃O₂ and N₂(O₂)₂. Stoichiometric compounds have now been observed in a large number of molecular binary mixtures under pressure since their first discovery with He(N₂)₁₁ (Ref. 6) and Ne(He)₂.⁷ The stability of these compounds has been explained in terms of efficient packing. In the present case, efficient packing¹¹ is probably not the only reason of the stability of the two compounds but also the magnetic and pairing interaction between O₂ molecules should play a role. Furthermore, in contrast to the observation of the Van der Waals compounds in the other molecular mixtures where the

structures of binary hard-sphere compounds or intermetallic compounds have been found, in the present case the two compounds should correspond to a special network arrangement in a substitutional solid solution. A more complete understanding of these compounds will require further work.

Finally, a phenomena of rapid recrystallization has been observed. This has been clearly measured from the change upon decreasing pressure of the x-ray diffraction patterns of the 66 mol% O₂ mixture. Starting in the $S2+S4$ domain of the binary phase diagram, in Fig. 1, a fine-grained polycrystalline mixture of almost pure β -O₂ and δ -N₂ with 35 mol% O₂ is observed. Then, by decreasing rapidly the pressure in the $S2$ domain around 7 GPa, a rapid growth of few single crystals occupying the whole sample chamber is observed within few minutes. That implies great mobility of the molecules, quite unexpected because the vacancy mechanism of diffusion should be inhibited essentially because the PV term is adding to the energy of vacancy formation. Furthermore, the spontaneous recrystallization in a single crystal of fine powders of the pure end components at the same pressure is never observed. A δ -N₂ powder will not spontaneously recrystallize in a single crystal, nor a β -O₂ powder. Consequently, it seems that this recrystallization effect is due to intrinsic properties of the mixture. A microscopic understanding of it would be very interesting because diffusion and recrystallization properties have been scarcely investigated by experiments above 1 GPa, despite their importance for the geochemistry of inner earth or material synthesis at high pressure. Further measurements are now needed.

V. CONCLUSIONS

The O₂/N₂ binary phase diagram is presented here at 295 K by the combination of three measurements: visual observation to observe the phase transitions; Raman spectroscopy of the vibrons of the two molecules to probe the crystal field on the molecules; x-ray determination of the structures of the solid solutions. This extends in accuracy and details a previous determination by Raman spectroscopy. The present study of the O₂/N₂ phase diagram brings the possibility to investigate differently the properties of the pure end members solid. A large solubility of O₂ in solid N₂ is observed whereas a small solubility of N₂ molecules in solid O₂ is observed. This dissymmetry of solubility can be ascribed to the magnetic interaction between O₂ molecules. And above 9 GPa, the pairing between O₂ molecules lessens further the amount of solubility of N₂ in pure O₂. That is stressing the role of magnetic interaction and of pairing to stabilize the structures of pure O₂. If these two interactions were turned off, the sequence of phase transition of pure N₂ would probably be observed in solid O₂ because, on the other side of the diagram, O₂ in solid N₂ is only slightly perturbing the sequence of phase transitions of the pure N₂ solid. Generally, the calculation of the boundary lines of the phase diagram is known to be a good test of the binary interaction. In the present case, such a calculation of the binary phase diagram can also be useful to test the description of magnetic and pairing interaction between O₂ molecules, which is still not completely understood.

Three potentially interesting extensions of the present structural study of O_2/N_2 solid solutions should be now investigated. First, the compression of a O_2/N_2 solid solution with 10 mol% O_2 could probably produce a metal in the 100 GPa range. N_2 has been observed to transform into a nonmolecular semiconducting phase at 140 GPa (Ref. 3) that remains until at least 240 GPa. But solid O_2 has been observed to become a metal at 96 GPa.¹⁹ The inclusion of O_2 impurity in N_2 solid in the 100 GPa range will be equivalent to putting a metal impurity in a semiconductor and hence should lower the insulator-metal transition of the pure system. An interesting question is also to know whether or not for an O_2 concentration below 20 mol% O_2 , the solid solution can become a metal before its transition to the nonmolecular phase. Second, the change of the magnetic property of the O_2 molecules under high pressure is a subject of current interest. As recently calculated,³¹ the O_2/N_2 solid solutions offer interesting different geometries to study the magnetic properties of O_2 clusters under pressure. Third, from high-pressure work done on N_2O_4 ,³² it can be estimated that

O_2/N_2 solid solution might become unstable with respect to $NO^+NO_3^-$ under pressure. Although there is no evidence of chemical change in the present work, it would be interesting to know at which pressure chemistry changes will be observed and if a heating of the sample can overcome the activation barrier of the reaction in the pressure range of the present study.

ACKNOWLEDGMENTS

We are grateful to the Air Liquide company for funding the Ph.D. of Davina Sihachakr. We are also grateful to M. Mezouar on ID30 and to M. Hanfland on ID09 to let us use extra beamtime at the ESRF for this project and for experimental help at the synchrotron. We thank A. Dewaele, R. Andre, L. R. Benedetti, S. Desgreniers, and G. Weck for experimental help and helpful discussions. Finally we thank M. Maksym Minenko and Hans Jodl for sending a preprint of their work during the writing up of the present paper.

¹R. J. Hemley, *Annu. Rev. Phys. Chem.* **51**, 763 (2000).

²G. Weck, P. Loubeyre, and R. LeToullec, *Phys. Rev. Lett.* **88**, 035504 (2002).

³M. Eremets, R. J. Hemley, H. K. Mao, and E. Gregorianz, *Nature (London)* **411**, 170 (2001).

⁴P. F. McMillan, *Nat. Mater.* **1**, 19 (2002).

⁵F. H. Ree, in *Simple Molecular Systems at Very High Density*, edited by A. Polian and P. Loubeyre (Plenum, New York, 1988), p. 153.

⁶W. L. Vos, L. W. Finger, R. J. Hemley, J. Z. Hu, H. K. Mao, and J. A. Schouten, *Nature (London)* **358**, 46 (1992).

⁷P. Loubeyre, M. Jean-Louis, R. LeToullec, and L. Charon-Gérard, *Phys. Rev. Lett.* **70**, 178 (1993).

⁸B. J. Baer and M. Nicol, *J. Phys. Chem.* **93**, 1683 (1989).

⁹B. J. Baer and M. Nicol, *J. Phys. Chem.* **94**, 1073 (1990).

¹⁰K. Damde and H. Jodl, *J. Low Temp. Phys.* **111**, 327 (1998).

¹¹P. Loubeyre, *High Press. Res.* **14**, 353 (1996).

¹²H. K. Mao, J. Xu, and P. M. Bell, *J. Geophys. Res.* **5**, 4673 (1986).

¹³A. P. Hammersley, S. O. Svensson, M. Hanfland, A. N. Fitch, and D. Häusermann, *High Press. Res.* **14**, 235 (1996).

¹⁴M. Nicol and W. B. Holzapfel, *Chem. Phys. Lett.* **68**, 49 (1979).

¹⁵B. Olinger, R. L. Mills, and R. B. Roof, Jr., *J. Chem. Phys.* **81**, 5068 (1984).

¹⁶D. Schiferl, D. T. Cromer, and R. L. Mills, *Acta Crystallogr., Sect. B: Struct. Crystallogr. Cryst. Chem.* **B37**, 1329 (1981).

¹⁷D. Schiferl, D. T. Cromer, L. A. Schwalbe, and R. L. Mills, *Acta Crystallogr., Sect. B: Struct. Sci.* **B39**, 153 (1983).

¹⁸H. d'Amour, W. B. Holzapfel, and M. Nicol, *J. Chem. Phys.* **85**, 130 (1981).

¹⁹S. Desgreniers, Y. K. Vohran, and A. L. Ruoff, *Bull. Am. Phys. Soc.* **33**, 521 (1985).

²⁰D. Schiferl, D. T. Cromer, R. R. Ryan, A. C. Larson, R. LeSar, and R. L. Mills, *Acta Crystallogr., Sect. C: Cryst. Struct. Commun.* **C39**, 1151 (1983).

²¹R. L. Mills, B. Olinger, and D. T. Cromer, *J. Chem. Phys.* **84**, 2837 (1986).

²²B. Olinger, *J. Chem. Phys.* **80**, 1309 (1984).

²³D. T. Cromer, R. L. Mills, D. Schiferl, and L. A. Schwalbe, *Acta Crystallogr., Sect. B: Struct. Crystallogr. Cryst. Chem.* **B37**, 8 (1981).

²⁴D. Schiferl, S. Buchsbaum, and R. L. Mills, *J. Phys. Chem.* **89**, 2324 (1985).

²⁵M. Hanfland, M. Lorenzen, C. Wassilew-Reul, and F. Zontone, *Rev. High Pressure Sci. Technol.* **7**, 787 (1998).

²⁶H. Schneider, W. Häfner, and A. Wokaun, *J. Chem. Phys.* **96**, 8046 (1992).

²⁷H. J. Jodl, F. Bolduan, and H. D. Hochheimer, *Phys. Rev. B* **31**, 7376 (1985).

²⁸L. Charon, P. Loubeyre, and M. Jean-Louis, *High Press. Res.* **8**, 399 (1991).

²⁹P. Loubeyre, in *Molecular Systems under High Pressure*, edited by R. Pucci and G. Piccitto (North-Holland, Amsterdam, 1991), p. 245.

³⁰M. Minenko, J. Kreutz, T. Hupprich, and H. Jodl (unpublished).

³¹Y. Freiman, S. Tretyak, and A. Jezowski, *J. Low Temp. Phys.* **26**, 1029 (2000).

³²Y. Song, M. Somayazulu, H. K. Mao, R. J. Hemley, and D. R. Herschbach, *J. Chem. Phys.* **118**, 8350 (2003).